forum acusticum 2026
8-12 September · Graz, Austria

OBTAINING POROELASTIC PARAMETERS OF POROUS MATERIALS FROM IMPEDANCE TUBE MEASUREMENTS

Florian Kraxberger[1], Alfonso Caiazzo[2], Giuseppe Petrone[2], Christian Adams[1]

[1] *Institute of Fundamentals and Theory in Electrical Engineering (IGTE), Graz University of Technology, Austria*
[2] *PASTA LAB — Laboratory for Promoting Experiences in Aeronautical Structures and Acoustics, University "Federico II" of Naples, Italy*

Abstract

The accurate characterization of the acoustic and elastic parameters of a porous material based on impedance tube measurements presents challenges, in particular, because the specimens' diameters can deviate from the nominal inner diameter of the impedance tube. If the specimen's diameter exceeds the nominal diameter of the tube, it is compressed and therefore the material parameters are modified. The elastic solid phase of the diphasic poroelastic material is modelled using Biot's model with the parameters mass density, Young's modulus, Poisson's ratio, and loss factor. In the fluid phase, viscous and thermal dissipation is modeled with the JCAL model which uses the parameters static airflow resistivity, open porosity, tortuosity, static thermal permeability, and viscous and thermal characteristic lengths. The model is restricted to plane waves at normal incidence, enabling an analytical coupling of the two models. In this contribution, the parameters of the diphasic poroelastic Biot-JCAL model are fitted to impedance tube measurements of the *FOAM 02*-database. This database contains 864 measurements of the sound absorption coefficient obtained in an impedance tube with $\pm 2\,\%$ diameter deviation. An inverse parameter characterisation model is implemented in Python. The results highlight the effect of diameter inaccuracies on the visco-thermal and elastic parameters of the Biot-JCAL model.

Keywords: *Acoustic absorption, poroelastic materials, Biot-JCAL*

1. Introduction

Knowledge of the acoustic properties of porous materials is essential for accurate predictions of their effect on the acoustic field [1], [2]. To do so, the impedance tube is a common tool to determine the acoustic properties of porous materials [3]. However, inaccuracies in specimen preparation may cause the actual specimen diameter to deviate from the nominal diameter of the impedance tube. On the one hand, if the specimen diameter is smaller than the nominal tube diameter, the leakage effects affect low frequencies in particular [4]. On the other hand, if the specimen diameter exceeds the nominal tube diameter, the specimen is compressed which can lead to local minima in the measured sound absorption coefficient (SAC) curve, see, e.g., [5], [6]. These local SAC minima can be attributed to an elastic motion of the skeleton material, following Biot's theory of a diphasic poroelastic materials [7], [8]. Thereby, the fluid phase (i.e., the fluid filling the pores) is considered to be air, and the elastic solid phase is considered acoustically sound hard, but somewhat elastically compliant to the impinging acoustic pressure and particle velocity. For the fluid phase, a common model to describe the visco-thermal dissipation is the Johnson–Champoux–Allard–Lafarge (JCAL) model, as described in [9], which has six parameters. The elastic solid phase is modelled with the diphasic Biot model [10], [11], which has an additional four parameters. Thus, the full model consists of ten parameters, as listed in Table 1.

In [5, Fig. 6], it is evident that the JCAL model alone is not able to reproduce the effects of the compression waves in the elastic solid. Thus, in this contribution, an auto-differentiable implementation of the diphasic Biot-JCAL model is proposed. The fluid and elastic solid parameters of this model are jointly fitted to impedance tube SAC measurements of the *FOAM 02*-dataset [13].

The paper is organised as follows. In section 2, the Biot-JCAL model is explained, followed by a discussion on the auto-differentiable implementation in Python, and a brief description of the *FOAM 02*-dataset. In section 3, the parameter fitting results are

Corresponding author: *kraxberger@turgaz.at.*

Table 1: Parameters of the Biot-JCAL model for poroelastic materials with typical ranges for poroelastic parameters. The initial value of the density ρ_0 is chosen based on the nominal material density $\bar{\rho}_0$, such that for melamine resin foam $\bar{\rho}_0 = 9\,\frac{\mathrm{kg}}{\mathrm{m}^3}$, and for the PET fibre plate $\bar{\rho}_0 = 50\,\frac{\mathrm{kg}}{\mathrm{m}^3}$ [5].

Parameter	Symbol	Typical range [12]	Initial value	SI Unit
JCAL model parameters (fluid phase)				
Static airflow resistivity	σ	$(1 \cdot 10^3,\, 1 \cdot 10^6)$	10 000.0	$\mathrm{Ns/m^4}$
Open porosity	ϕ	$(0.5, 0.99)$	0.94	—
High frequency limit of the tortuosity	α_∞	$(1.0,\, 3.0)$	1.06	—
Viscous characteristic length	Λ	$(11 \cdot 10^{-6},\, 350 \cdot 10^{-6})$	$56 \cdot 10^{-6}$	m
Thermal characteristic length	Λ'	$(11 \cdot 10^{-6},\, 350 \cdot 10^{-6})$	$140 \cdot 10^{-6}$	m
Static thermal permeability	k_0'	$(1 \cdot 10^{-10},\, 1 \cdot 10^{-8})$	$23 \cdot 10^{-10}$	m^2
Biot model parameters (elastic solid phase)				
Mass density	ρ_1	> 0	$\bar{\rho}_0$	$\frac{\mathrm{kg}}{\mathrm{m}^3}$
Young's modulus	E	$(10,\, 1 \cdot 10^9)$	$4 \cdot 10^5$	Pa
Poisson's ratio	ν	$(0,\, 0.5)$	0.25	—
Loss factor	η_s	$(1 \cdot 10^{-2},\, 1)$	0.2	—

discussed. Finally, section 4 provides a conclusion and outlook.

2. Methods and Materials

2.1. Biot-JCAL Model for Poroelastic Materials

The simplified Biot-JCAL model employed in this work assumes just compression waves in the material and no shear wave, which makes it a useful tool for computing the SAC curve because of the one-dimensional nature of the compression waves.

Fluid Phase. According to the JCAL model, the frequency-dependent equivalent mass density $\rho_{\mathrm{eq}}(\omega, \boldsymbol{\theta}_{\mathrm{JCAL}})$ and bulk modulus $K_{\mathrm{eq}}(\omega, \boldsymbol{\theta}_{\mathrm{JCAL}})$ are

$$\rho_{\mathrm{eq}}(\omega, \boldsymbol{\theta}_{\mathrm{JCAL}}) = \frac{\alpha_\infty \rho_0}{\phi} A\,, \tag{1}$$

$$K_{\mathrm{eq}}(\omega, \boldsymbol{\theta}_{\mathrm{JCAL}}) = \frac{\gamma p_0 / \phi}{\gamma - (\gamma - 1) B^{-1}}\,, \tag{2}$$

with the angular frequency $\omega = 2\pi f$ and the short-hands

$$A = 1 - \mathrm{j}\frac{\phi\sigma}{\omega\rho_0\alpha_\infty}\sqrt{1 + \mathrm{j}\frac{4\alpha_\infty^2 \eta_0 \rho_0 \omega}{\sigma^2 \Lambda^2 \phi^2}}\,, \tag{3}$$

$$B = 1 - \mathrm{j}\frac{\phi\kappa}{\omega\rho_0 k_0' C_{\mathrm{p}}}\sqrt{1 + \mathrm{j}\frac{4 k_0'^2 C_{\mathrm{p}} \rho_0 \omega}{\kappa \Lambda'^2 \phi^2}}\,, \tag{4}$$

where the parameters of the JCAL model as listed in Table 1 are summarized in the parameter vector $\boldsymbol{\theta}_{\mathrm{JCAL}} = [\sigma, \phi, \alpha_\infty, \Lambda, \Lambda', k_0']^\top$. The constitutive parameters of air are the ambient density ρ_0, the isentropic exponent γ, the dynamic viscosity η_0, the specific heat at constant ambient pressure C_{p} and the thermal conductivity κ. These are evaluated according to [12] at the ambient temperature $T_0 = 20.0\,°\mathrm{C}$. Therewith, the bulk modulus of the proportion of the fluid phase can be computed with $K_{\mathrm{e}} = \phi K_{\mathrm{eq}}$.

Elastic Solid Phase. The effective mass densities in the solid phase are defined as [10], [11]

$$\begin{aligned} \tilde{\rho}_{22} &= \rho_{\mathrm{eq}}\phi^2\,, \qquad \tilde{\rho}_{12} = \phi\rho_0 - \rho_{\mathrm{eq}}\phi^2\,, \\ \tilde{\rho}_{11} &= \rho_{\mathrm{eq}}\phi^2 - \phi\rho_0 + \rho_1\,, \\ \tilde{\rho}_{\mathrm{s}} &= \tilde{\rho}_{11} - \tilde{\rho}_{12}^2 / \tilde{\rho}_{22} \end{aligned} \tag{5}$$

The shear modulus N and the bulk modulus K_{b} of the solid are evaluated with [9, Eq. (6.29)]

$$N = \frac{E(1 + \mathrm{j}\eta_s)}{2(\nu + 1)}\,, \qquad K_{\mathrm{b}} = \frac{2N(1 + \nu)}{3(1 - 2\nu)}\,, \tag{6}$$

from which the dynamic coefficients of elasticity $\tilde{P}$, $\tilde{Q}$, and $\tilde{R}$ can be obtained [9, Eq. (6.26)–(6.28)]

$$\begin{aligned} \tilde{P} &= \frac{(1 - \phi)^2}{\phi} K_{\mathrm{e}} + K_{\mathrm{b}} + \frac{4N}{3}\,, \\ \tilde{Q} &= (1 - \phi) K_{\mathrm{e}}\,, \qquad \tilde{R} = \phi K_{\mathrm{e}}\,. \end{aligned} \tag{7}$$

Two compressional waves are observed: the dilatational wave and the rotational wave. In ordinary fluid-saturated porous materials, these can be interpreted as a frame-born wave and an airborne wave [9, Sec. 6.5.3]. Only normally incident plane waves are considered, therefore shear waves can be neglected. Now, the complex wave numbers of the compressional waves δ_1 and δ_2 can be computed, respectively, with [9, Eq. (6.67)–(6.68)]

$$\begin{aligned} \delta_1 &= \sqrt{\frac{\omega^2 \left[\tilde{P}\tilde{\rho}_{22} + \tilde{R}\tilde{\rho}_{11} - 2\tilde{Q}\tilde{\rho}_{12} - \sqrt{\Delta}\right]}{2\left(\tilde{P}\tilde{R} - \tilde{Q}^2\right)}}\,, \\ \delta_2 &= \sqrt{\frac{\omega^2 \left[\tilde{P}\tilde{\rho}_{22} + \tilde{R}\tilde{\rho}_{11} - 2\tilde{Q}\tilde{\rho}_{12} + \sqrt{\Delta}\right]}{2\left(\tilde{P}\tilde{R} - \tilde{Q}^2\right)}}\,. \end{aligned} \tag{8}$$

Therein, Δ is a short-hand notation for [9, Eq. (6.69)]

$$\begin{aligned} \Delta = {} & \left[\tilde{P}\tilde{\rho}_{22} + \tilde{R}\tilde{\rho}_{11} - 2\tilde{Q}\tilde{\rho}_{12}\right]^2 \\ & - 4\left(\tilde{P}\tilde{R} - \tilde{Q}^2\right)\left(\tilde{\rho}_{11}\tilde{\rho}_{22} - \tilde{\rho}_{12}^2\right)\,. \end{aligned} \tag{9}$$

The ratios between the velocity of air over the velocity of the skeleton of the two compressional waves are given by [9, Eq. (6.71)]

$$\frac{c_i^{\mathrm{f}}}{c_i^{\mathrm{s}}} = \mu_i = \frac{\tilde{P}\delta_i^2 - \omega^2\tilde{\rho}_{11}}{\omega^2\tilde{\rho}_{12} - \tilde{Q}\delta_i^2}\,, \qquad i = 1,2\,. \tag{10}$$

For each of the two compressional waves, one characteristic impedance of air and one of the frame can be defined, such that four characteristic impedances arise in total as [9, Eq. (6.74)–(6.77)]

$$\begin{aligned} Z_i^{\mathrm{f}} &= \left(\tilde{R} + \frac{\tilde{Q}}{\mu_i}\right)\frac{\delta_i}{\phi\omega}\,, \qquad i = 1,2 \\ Z_i^{\mathrm{s}} &= \left(\tilde{R} + \tilde{Q}\mu_i\right)\frac{\delta_i}{\omega}\,, \qquad i = 1,2\,. \end{aligned} \tag{11}$$

Sound Absorption Coefficient. The surface impedance W of the diphasic poroelastic material for normal incident waves can be computed with [9, Eq. (6.107)–(6.108)]

$$W = -\mathrm{j}\,\frac{Z_1^{\mathrm{s}} Z_2^{\mathrm{f}}\mu_2 - Z_2^{\mathrm{s}} Z_1^{\mathrm{f}}\mu_1}{D}\,, \tag{12}$$

where

$$\begin{aligned} D = {}& (1-\phi+\phi\mu_2)\left[Z_1^{\mathrm{s}} - (1-\phi)Z_1^{\mathrm{f}}\mu_1\right]\tan\delta_2 t + \\ &+ (1-\phi+\phi\mu_1)\left[Z_2^{\mathrm{s}}\mu_2(1-\phi) - Z_2^{\mathrm{s}}\right]\tan\delta_1 t\,. \end{aligned} \tag{13}$$

Finally, the SAC can be computed with

$$\alpha_{\mathrm{BiotJCAL}}(\omega) = 1 - \left|\frac{W(\omega) - Z_0}{W(\omega) + Z_0}\right|^2\,. \tag{14}$$

Forward Model. By introducing the Biot parameter vector $\boldsymbol{\theta}_{\mathrm{Biot}} = [\rho_1, E, \nu, \eta_s]^\top$, equations (1) to (14) can be formulated as a forward model for the sound absorption coefficient that only depends on the frequency and the parameters of the Biot-JCAL model[1], such that

$$\alpha_{\mathrm{BiotJCAL}}(\omega) = f(\omega, \boldsymbol{\theta}_{\mathrm{JCAL}}, \boldsymbol{\theta}_{\mathrm{Biot}})\,. \tag{15}$$

2.2. Implementation with PyTorch Auto-Differentiation

In [12], among concise explanations of the material model, a *Matlab* code is available, in which the forward model is implemented. This was used as a basis for the forward-model implementation in Python, which computes the frequency-dependent SAC from the $\boldsymbol{\theta}_{\mathrm{JCAL}}$ and $\boldsymbol{\theta}_{\mathrm{Biot}}$ using complex-valued PyTorch tensor operations. The inverse identification of the Biot–JCAL parameters was implemented as a fully differentiable optimization problem in PyTorch [14]. All model quantities are represented as `torch.Tensor` objects, enabling automatic differentiation of the scalar loss with respect to the material parameters.

[1] It is assumed that the constitutive parameters of air are known and constant.

The full parameter vector $\boldsymbol{\theta}$ is composed of the JCAL and Biot parameters, such that $\boldsymbol{\theta} = \left[\boldsymbol{\theta}_{\mathrm{JCAL}}^\top, \boldsymbol{\theta}_{\mathrm{Biot}}^\top\right]^\top$. Instead of optimizing these physical parameters directly, unconstrained variables $z_i \in \mathbb{R}$ are optimized and mapped to bounded physical parameters by a sigmoid function. Thus, the constraint physical parameters are mapped to an unconstrained value range in the optimization hyperspace, which is advantageous for the optimizer. For example, the i-th element of $\boldsymbol{\theta}$ is transformed as follows

$$\theta_i = \theta_{i,\min} + \mathrm{sigmoid}(z_i)\left(\theta_{i,\max} - \theta_{i,\min}\right)\,, \tag{16}$$

where $\theta_{i,\max}$ and $\theta_{i,\min}$ are the maximum and minimum of the search interval of parameter θ_i, as defined in Table 1. The constraint $\Lambda \leq \Lambda'$ is enforced directly in the parameter transformation by making the lower bound of Λ' depend on the current value of Λ.

For each selected specimen configuration, multiple measured SAC curves are preprocessed and averaged. The optimization minimizes a weighted mean-squared error between the simulated and averaged measured absorption coefficient, such that the loss $\mathcal{L}$ reads

$$\mathcal{L} = \frac{1}{N_{\mathrm{freq}}}\sum_{j=1}^{N_{\mathrm{freq}}} w_j\left(\alpha_{\mathrm{BiotJCAL}}(\omega_j) - \alpha_{\mathrm{meas}}(\omega_j)\right)^2\,. \tag{17}$$

Frequency-dependent weights w_j are used to emphasize selected frequency bands. This is used to emphasize the loss in the frequency interval $f \in [400, 800]\,\mathrm{Hz}$ by a factor of 10, because in this frequency interval, the local minima in the SAC curve contain relevant information regarding the effect elastic wave motion, as it can be seen in Figure 1. The minimization is performed with `torch.optim.LBFGS`. The required closure evaluates the differentiable forward model for $\alpha_{\mathrm{BiotJCAL}}$, computes the loss $\mathcal{L}$, calls the PyTorch auto-differentiation function `backward()`, and returns the scalar loss to the optimizer. Gradients are therefore obtained by PyTorch automatic differentiation. To reduce sensitivity to local minima, the inverse parameter identification was performed using a deterministic multi-start strategy. For each specimen configuration, the LBFGS optimization was repeated from 27 initial parameter sets generated by scaling the initial values of the flow resistivity σ, mass density ρ_1, and Young's modulus E according to $\sigma \in \{0.5, 1.0, 2.0\}\sigma_0$, $\rho_1 \in \{0.8, 1.0, 1.2\}\rho_{1,0}$, and $E \in \{0.3, 1.0, 3.0\}E_0$. All other parameters were initialized solely at the values listed in Table 1. The final parameter set was selected as the solution with the lowest loss among all starts, while all optimizations used identical bounds and LBFGS settings.

2.3. Dataset Description

In this contribution, the *FOAM 02* dataset is used, for which a detailed description is available [5]. The dataset is openly available at [13]. It contains sound absorption curve (SAC) measurements of specimens with the following specifications:

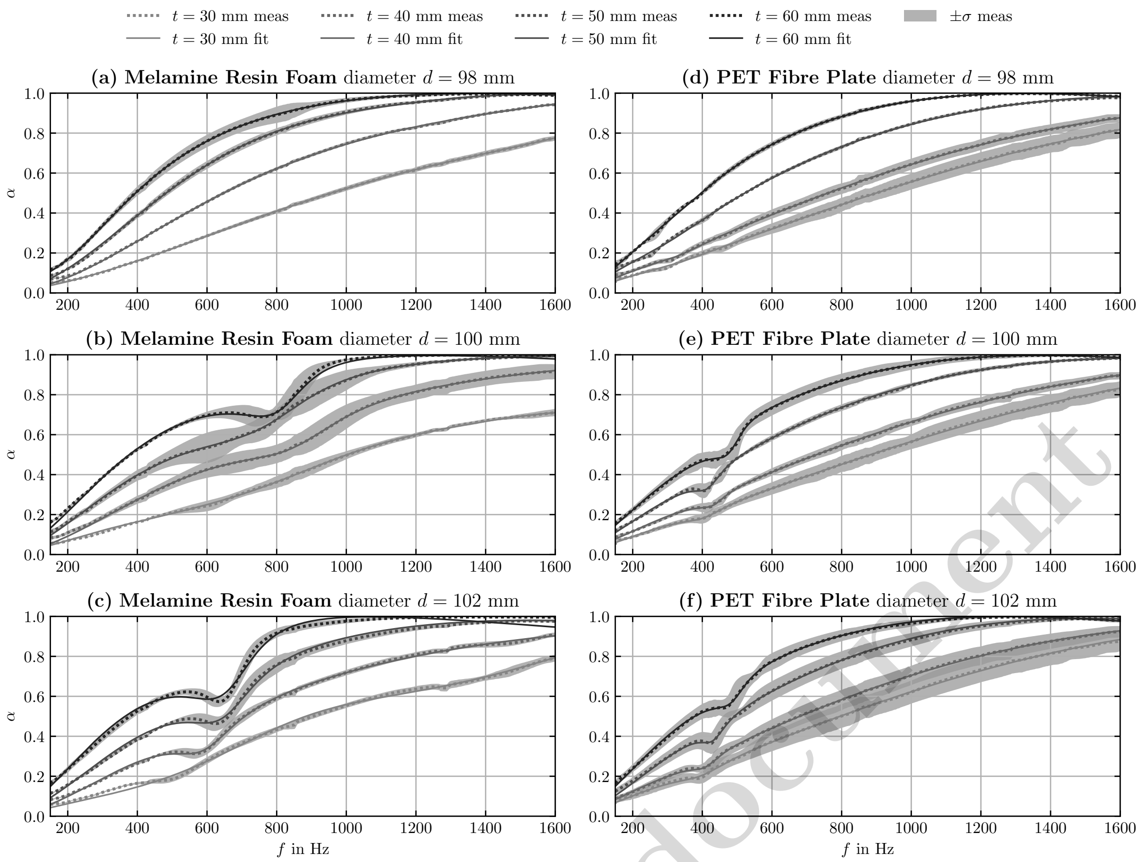

Figure 1: Averaged measured SAC curves and results of the Biot-JCAL fitting procedure for the two materials, four thicknesses, and three diameters. The shaded area represents the standard deviation σ of the averaged measured SAC curves.

- **2 materials:** Melamine resin foam (*Basotect* with a nominal density of $\bar{\rho}_1 = 9\,\frac{\mathrm{kg}}{\mathrm{m}^3}$) and PET fibre plates (*Pinta Plano Polar* with a nominal density of $\bar{\rho}_1 = 50\,\frac{\mathrm{kg}}{\mathrm{m}^3}$)
- **3 diameters:** $d \in \{98, 100, 102\}\,\mathrm{mm}$
- **4 thicknesses:** $t \in \{30, 40, 50, 60\}\,\mathrm{mm}$
- **4 rotational angles:** $\beta \in \{0, 90, 180, 270\}\,^\circ$ The rotational angle describes a rotation of the specimen relative to the impedance tube, as described in [5].

This results in 96 possible parameter combinations, as described in [5]. For each parameter combination of material, diameter and thickness, 3 specimens have been manufactured with the cutting device described in [5], thus 72 specimens have been manufactured, and each measurement is performed with three repetitions. In total, 2 materials $\cdot$ 3 diameters $\cdot$ 4 thicknesses $\cdot$ 3 specimens $\cdot$ 4 rotational angles $\cdot$ 3 repetitions $= 864$ SAC curves make up the *FOAM 02* dataset. For this paper, the SAC curves are averaged across the same specimens, repetition measurements and rotational angles, because these factors do not impact the SAC measurement significantly [6]. Hence, 24 SAC curves are considered.

3. Results

In Figure 1, the results of the Biot-JCAL fit is depicted for both materials. Table 2 shows the parameters of the Biot-JCAL model for melamine resin foam. In Table 3, the Biot-JCAL parameters are listed for PET fibre plates. To evaluate the overall agreement between fitted and measured SAC curves, the final loss $\mathcal{L}$ of the optimized parameter set is also reported in Table 2 and Table 3. The evolution of the optimized parameters over diameter variations is depicted in Figure 2. In Figure 2, it can be seen, that a variation of the diameter induces a correlating change of some parameters. For example, σ tends to decrease with increasing specimen diameters in Figure 2a. Another example is given by the overall increase of ϕ with increasing diameters, which can be observed in Figure 2b.

4. Conclusion

The proposed inverse-identification procedure provides generally good agreement between the measured and fitted sound absorption coefficient curves, as it can be observed in Figure 1. This is quantified by low values of the loss function for most configurations in Table 2 and Table 3. The main discrepancies are observed for the melamine resin foam specimens with a diameter

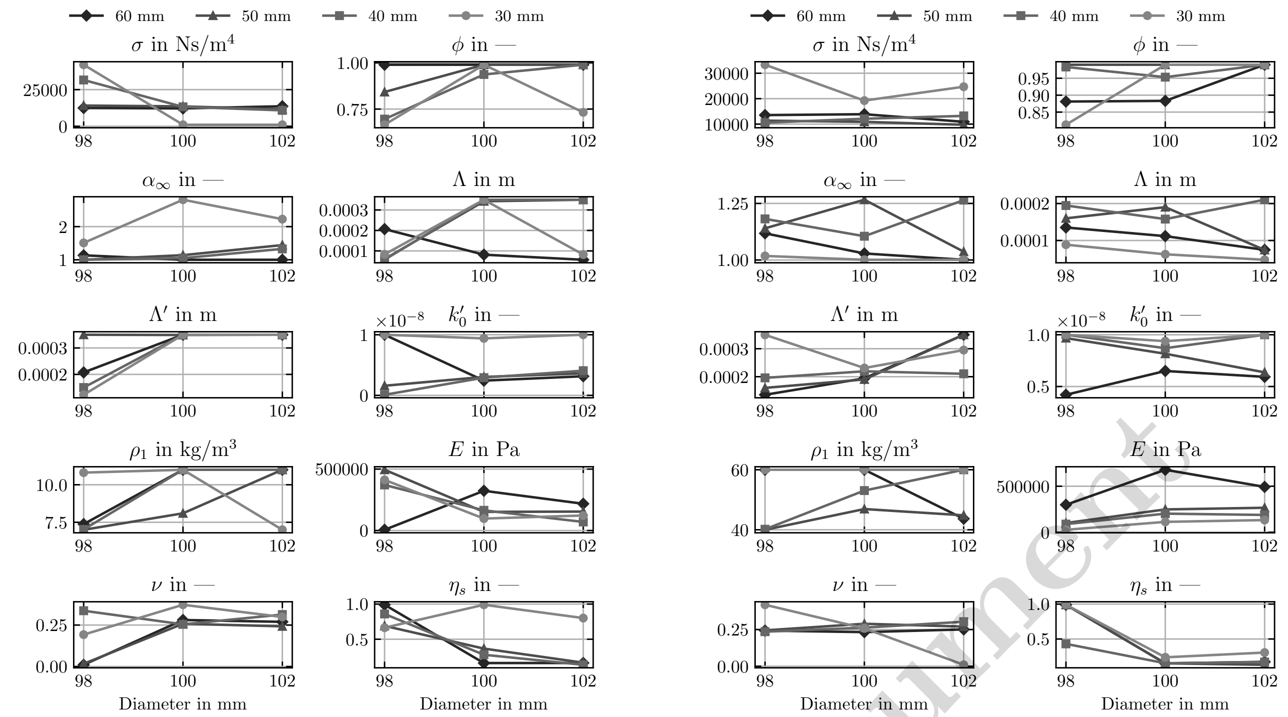

(a) Melamine resin foam. **(b)** PET fibre plate.

Figure 2: Evolution of Biot-JCAL parameters over diameter variations.

of $d = 102\,\text{mm}$ and thicknesses of $t = 60\,\text{mm}$. The variation in the evolution of the Biot-JCAL parameter depicted in Figure 2 is contributes to understanding the cause-effect relation between specimen diameter and measured SAC. However, it still needs validation through uncertainty considerations. Compared to the JCAL model used in [5], the Biot-JCAL formulation improves the prediction of the local minima associated with the elastic motion of the material skeleton, indicating that specimen compression can influence both the visco-thermal and elastic response of porous materials. Nevertheless, the identified parameters should be interpreted with caution because of the non-unique nature of the ten-parameter inverse problem. Future work will therefore focus on parameter sensitivity, identifiability, and uncertainty quantification.

5. Acknowledgments

F. K. and Ch. A. received funding from the ”BMIMI Endowed Professorship on Noise Impact Research: Competence Center for Traffic Noise and Health” of the Austrian Research Promotion Agency (FFG) under project No. FO999891611. The authors thank Paul Bereuter of IEM Graz, for the elegant idea to use an auto-differentiable PyTorch model.

References

[1] M. Vorländer, “Computer simulations in room acoustics: Concepts and uncertainties,” *The Journal of the Acoustical Society of America*, vol. 133, no. 3, pp. 1203–1213, Mar. 2013. DOI: 10.1121/1.4788978.

[2] F. Kraxberger, E. Kurz, W. Weselak, G. Kubin, M. Kaltenbacher, and S. Schoder, “A validated finite element model for room acoustic treatments with edge absorbers,” *Acta Acustica*, vol. 7, p. 48, Oct. 2023. DOI: 10.1051/aacus/2023044.

[3] N. Hiremath, V. Kumar, N. Motahari, and D. Shukla, “An Overview of Acoustic Impedance Measurement Techniques and Future Prospects,” *Metrology*, vol. 1, no. 1, pp. 17–38, May 2021. DOI: 10.3390/metrology1010002.

[4] A. Cummings, “Impedance tube measurements on porous media: The effects of air-gaps around the sample,” *Journal of Sound and Vibration*, vol. 151, no. 1, pp. 63–75, Nov. 1991. DOI: 10.1016/0022-460X(91)90652-Z.

[5] A. Caiazzo, F. Kraxberger, A. Wurzinger, J. Boysen, G. Petrone, S. Schoder, S. De Rosa, M. Kaltenbacher, and C. Adams, “FOAM 02: A dataset of impedance tube measurements with different materials and diameter variations,” *Acta Acustica*, vol. 9, no. 50, p. 13, Jul. 2025. DOI: 10.1051/aacus/2025033.

[6] A. Caiazzo, F. Kraxberger, G. Petrone, S. De Rosa, and C. Adams, “Identifying sources of variability in impedance tube sound absorption measurements with multivariate explainable ma-

Table 2: Inversely determined parameters of the Biot-JCAL model for Melamine Resin Foam. Values are rounded to three significant digits.

Specimen		JCAL (fluid) parameters						Biot (elastic solid) parameters				Loss
t mm	d mm	σ Ns/m^4	ϕ —	α_∞ —	Λ m	Λ' m	k'_0 —	ρ_1 kg/m^3	E Pa	ν —	η_s —	$\mathcal{L}$ —
30	98	$4.20 \cdot 10^{4}$	0.665	1.51	$8.32 \cdot 10^{-5}$	$1.23 \cdot 10^{-4}$	$1.00 \cdot 10^{-8}$	10.8	$4.12 \cdot 10^{5}$	0.192	0.664	$9.00 \cdot 10^{-6}$
40	98	$3.16 \cdot 10^{4}$	0.696	1	$5.72 \cdot 10^{-5}$	$1.50 \cdot 10^{-4}$	$1.00 \cdot 10^{-10}$	7.02	$3.71 \cdot 10^{5}$	0.336	0.859	$1.61 \cdot 10^{-5}$
50	98	$1.41 \cdot 10^{4}$	0.842	1	$6.02 \cdot 10^{-5}$	$3.50 \cdot 10^{-4}$	$1.59 \cdot 10^{-9}$	7	$4.94 \cdot 10^{5}$	0.0164	0.69	$1.83 \cdot 10^{-5}$
60	98	$1.25 \cdot 10^{4}$	0.99	1.14	$2.07 \cdot 10^{-4}$	$2.08 \cdot 10^{-4}$	$1.00 \cdot 10^{-8}$	7.38	$6.09 \cdot 10^{3}$	0.0104	0.99	$8.14 \cdot 10^{-6}$
30	100	$1.00 \cdot 10^{3}$	0.99	2.81	$3.50 \cdot 10^{-4}$	$3.50 \cdot 10^{-4}$	$9.40 \cdot 10^{-9}$	11	$9.75 \cdot 10^{4}$	0.372	0.99	$5.52 \cdot 10^{-5}$
40	100	$1.32 \cdot 10^{4}$	0.937	1.05	$3.50 \cdot 10^{-4}$	$3.50 \cdot 10^{-4}$	$2.93 \cdot 10^{-9}$	11	$1.64 \cdot 10^{5}$	0.254	0.279	$3.65 \cdot 10^{-5}$
50	100	$1.35 \cdot 10^{4}$	0.99	1.14	$3.42 \cdot 10^{-4}$	$3.49 \cdot 10^{-4}$	$3.05 \cdot 10^{-9}$	8.1	$1.52 \cdot 10^{5}$	0.258	0.366	$4.58 \cdot 10^{-5}$
60	100	$1.22 \cdot 10^{4}$	0.99	1	$8.16 \cdot 10^{-5}$	$3.50 \cdot 10^{-4}$	$2.44 \cdot 10^{-9}$	11	$3.23 \cdot 10^{5}$	0.281	0.161	$1.24 \cdot 10^{-4}$
30	102	$1.00 \cdot 10^{3}$	0.732	2.22	$8.21 \cdot 10^{-5}$	$3.50 \cdot 10^{-4}$	$1.00 \cdot 10^{-8}$	7	$1.22 \cdot 10^{5}$	0.299	0.801	$3.47 \cdot 10^{-4}$
40	102	$1.08 \cdot 10^{4}$	0.99	1.33	$3.50 \cdot 10^{-4}$	$3.50 \cdot 10^{-4}$	$4.07 \cdot 10^{-9}$	11	$6.99 \cdot 10^{4}$	0.313	0.136	$1.28 \cdot 10^{-4}$
50	102	$1.16 \cdot 10^{4}$	0.99	1.44	$3.50 \cdot 10^{-4}$	$3.50 \cdot 10^{-4}$	$3.63 \cdot 10^{-9}$	11	$1.54 \cdot 10^{5}$	0.242	0.166	$5.15 \cdot 10^{-4}$
60	102	$1.36 \cdot 10^{4}$	0.99	1	$5.67 \cdot 10^{-5}$	$3.50 \cdot 10^{-4}$	$3.15 \cdot 10^{-9}$	11	$2.18 \cdot 10^{5}$	0.269	0.162	0.0014

Table 3: Inversely determined parameters of the Biot-JCAL model for PET Fibre Plate. Values are rounded to three significant digits.

Specimen		JCAL (fluid) parameters						Biot (elastic solid) parameters				Loss
t mm	d mm	σ Ns/m^4	ϕ —	α_∞ —	Λ m	Λ' m	k'_0 —	ρ_1 kg/m^3	E Pa	ν —	η_s —	$\mathcal{L}$ —
30	98	$3.33 \cdot 10^{4}$	0.813	1.02	$8.86 \cdot 10^{-5}$	$3.50 \cdot 10^{-4}$	$1.00 \cdot 10^{-8}$	60	$2.65 \cdot 10^{4}$	0.419	0.99	$4.18 \cdot 10^{-5}$
40	98	$1.06 \cdot 10^{4}$	0.983	1.18	$1.95 \cdot 10^{-4}$	$1.96 \cdot 10^{-4}$	$1.00 \cdot 10^{-8}$	40.2	$8.82 \cdot 10^{4}$	0.235	0.431	$2.16 \cdot 10^{-5}$
50	98	$1.14 \cdot 10^{4}$	0.99	1.14	$1.60 \cdot 10^{-4}$	$1.60 \cdot 10^{-4}$	$9.67 \cdot 10^{-9}$	40	$9.99 \cdot 10^{4}$	0.244	0.99	$2.43 \cdot 10^{-5}$
60	98	$1.35 \cdot 10^{4}$	0.881	1.12	$1.35 \cdot 10^{-4}$	$1.35 \cdot 10^{-4}$	$4.20 \cdot 10^{-9}$	60	$2.98 \cdot 10^{5}$	0.243	0.99	$7.94 \cdot 10^{-6}$
30	100	$1.92 \cdot 10^{4}$	0.99	1	$6.27 \cdot 10^{-5}$	$2.31 \cdot 10^{-4}$	$9.38 \cdot 10^{-9}$	60	$1.13 \cdot 10^{5}$	0.258	0.238	$1.38 \cdot 10^{-5}$
40	100	$1.21 \cdot 10^{4}$	0.953	1.11	$1.58 \cdot 10^{-4}$	$2.19 \cdot 10^{-4}$	$8.70 \cdot 10^{-9}$	53.1	$2.02 \cdot 10^{5}$	0.263	0.153	$1.21 \cdot 10^{-5}$
50	100	$1.09 \cdot 10^{4}$	0.99	1.27	$1.90 \cdot 10^{-4}$	$1.90 \cdot 10^{-4}$	$8.16 \cdot 10^{-9}$	46.9	$2.48 \cdot 10^{5}$	0.289	0.152	$2.05 \cdot 10^{-5}$
60	100	$1.39 \cdot 10^{4}$	0.883	1.03	$1.12 \cdot 10^{-4}$	$1.94 \cdot 10^{-4}$	$6.50 \cdot 10^{-9}$	60	$6.79 \cdot 10^{5}$	0.233	0.151	$3.78 \cdot 10^{-5}$
30	102	$2.47 \cdot 10^{4}$	0.99	1	$4.78 \cdot 10^{-5}$	$2.95 \cdot 10^{-4}$	$1.00 \cdot 10^{-8}$	60	$1.32 \cdot 10^{5}$	0.009 58	0.306	$3.95 \cdot 10^{-5}$
40	102	$1.32 \cdot 10^{4}$	0.99	1.26	$2.10 \cdot 10^{-4}$	$2.10 \cdot 10^{-4}$	$1.00 \cdot 10^{-8}$	60	$1.88 \cdot 10^{5}$	0.303	0.171	$2.11 \cdot 10^{-5}$
50	102	$9.74 \cdot 10^{3}$	0.99	1.04	$7.44 \cdot 10^{-5}$	$3.50 \cdot 10^{-4}$	$6.37 \cdot 10^{-9}$	44.8	$2.66 \cdot 10^{5}$	0.27	0.131	$8.72 \cdot 10^{-5}$
60	102	$1.09 \cdot 10^{4}$	0.99	1	$7.47 \cdot 10^{-5}$	$3.50 \cdot 10^{-4}$	$5.93 \cdot 10^{-9}$	43.7	$4.93 \cdot 10^{5}$	0.251	0.173	$4.19 \cdot 10^{-5}$

chine learning," *Journal of Sound and Vibration*, Jul. 2026, Article in Press.

[7] M. A. Biot, "Theory of Propagation of Elastic Waves in a Fluid-Saturated Porous Solid. I. Low-Frequency Range," *The Journal of the Acoustical Society of America*, vol. 28, no. 2, pp. 168–178, Mar. 1956. DOI: 10.1121/1.1908239.

[8] M. A. Biot, "Theory of Propagation of Elastic Waves in a Fluid-Saturated Porous Solid. II. Higher Frequency Range," *The Journal of the Acoustical Society of America*, vol. 28, no. 2, pp. 179–191, Mar. 1956. DOI: 10.1121/1.1908241.

[9] J. F. Allard and N. Atalla, *Propagation of Sound in Porous Media: Modelling Sound Absorbing Materials*, 1st ed. Wiley, Oct. 2009. DOI: 10.1002/9780470747339.

[10] O. Dazel, F.-X. Bécot, and L. Jaouen, "Biot Effects for Sound Absorbing Double Porosity Materials," *Acta Acustica united with Acustica*, vol. 98, no. 4, pp. 567–576, Jul. 2012. DOI: 10.3813/AAA.918538.

[11] F.-X. Bécot and L. Jaouen, "An alternative Biot's formulation for dissipative porous media with skeleton deformation," *The Journal of the Acoustical Society of America*, vol. 134, no. 6, pp. 4801–4807, Dec. 2013. DOI: 10.1121/1.4826175.

[12] L. Jaouen, *APMR: Acoustical Porous Material Recipes — Biot's theory of poroelasticity*, Jul. 2026. [Online]. Available: https://apmr.matelys.com/PropagationModels/BiotTheory/.

[13] A. Caiazzo, F. Kraxberger, C. Adams, A. Wurzinger, G. Petrone, S. Schoder, S. De Rosa, and M. Kaltenbacher, *FOAM 02: Impedance tube measurements of two porous materials with diameter variation*, Nov. 2024. DOI: 10.5281/ZENODO.14190551.

[14] A. Paszke et al., "PyTorch: An imperative style, high-performance deep learning library," in *NEURIPS: Advances in neural information processing systems*, H. Wallach, H. Larochelle, A. Beygelzimer, F. dAlché-Buc, E. Fox, and R. Garnett, Eds., vol. 32, 2019.